in some of the fields surveyed, for instance, several commercial hybrids from Kolar district. Testing the leaf samples using indirect DAC–ELISA revealed the varying levels of virus concentrations. ToLCBV antiserum was more efficient than ToLCBV rCP antiserum in detection of virus in field collected samples (Table 1) Devaraja *et al.*[13] successfully produced monoclonal antibodies to ToLCBV and detected begomovirus infections in tomato samples, and other crop and weed species.

Polyclonal antibodies produced using purified intact virus and rCP of ToLCBV presented here clearly demonstrate the utility of the antisera in begomovirus detection in field samples and reservoir hosts.

1. Saikia, A. K. and Muniyappa, V., Epidemiology and control of tomato leaf curl virus in Southern India. *Trop. Agric.*, 1989, **66**, 350–354.
2. Ramappa, H. K., Muniyappa, V. and Colvin, J., The contribution of tomato and alternative host plants in leaf curl virus inoculum pressure in different areas of South India. *Ann. Appl. Biol.*, 1998, **133**, 187–198.
3. Muniyappa, V. *et al.*, Tomato leaf curl virus from Bangalore (ToLCV-Ban4): Sequence comparison with Indian ToLCV isolates, detection in plants and insects, and vector relationships. *Arch. Virol.*, 2000, **145**, 1583–1598.
4. Stein, V. E., Coutts, R. H. A. and Buck, K. W., Serological studies on tomato golden mosaic a geminivirus. *J. Gen. Virol.*, 1983, **64**, 2493–2498.
5. Sequeria, J. C. and Harrison, B. D., Serological studies on cassava latent virus. *Ann. Appl. Biol.*, 1982, **101**, 33–42.
6. Mathew, A. V. and Muniyappa, V., Purification and characterization of Indian cassava mosaic virus. *J. Phytopathol.*, 1992, **135**, 299–308.
7. Gugerli, P. and Fries, P., Characterization of monoclonal antibodies to potato virus-Y and their use for virus detection. *J. Gen. Virol.*, 1983, **64**, 2471–2477.
8. Muniyappa, V., Swanson, M. M., Duncan, G. H. and Harrison, B. D., Particle purification, properties, and epitope variability of Indian tomato leaf curl geminivirus. *Ann. Appl. Biol.*, 1991, **118**, 595–604.
9. Khan, J. A., Aminuddin, Raj, S. K. and Singh, B. P., Detection of plant viruses – biotechnological and molecular advances. *Indian J. Exp. Biol.*, 1998, **36**, 546–552.
10. Macintosh, S., Robinson, D. J. and Harrison, B. D., Detection of three whitefly transmitted geminiviruses in Europe by tests with heterologous monoclonal antibodies. *Ann. Appl. Biol.*, 1992, **121**, 297–303.
11. Kirthi, N. and Savithri, H. S., A conserved zinc finger motif in the coat protein of tomato leaf curl virus is responsible for binding to ssDNA. *Arch. Virol.*, 2003, **148**, 2369–2380.
12. Hobbs, H. A., Reddy, D. V. R., Rajeshwari, R. and Reddy, A. S., Use of direct antigen coating and protein – A coating ELISA procedure for detection of three peanut viruses. *Plant Dis.*, 1987, **71**, 747–749.
13. Devaraja, Gangatirkar, P., Sunitha, S. N., Narayanaswamy, K., Karande, A., Muniyappa, V. and Savithri, H. S., Production of monoclonal antibodies to *Tomato leaf curl Bangalore virus*. *Ann. Appl. Biol.*, 2004, **144**, 333–338.

ACKNOWLEDGEMENT. We thank the Department of Biotechnology, New Delhi for financial support.

Received 31 May 2003; revised accepted 1 February 2005

Ground penetrating radar studies of a point-bar in the Mahi River Basin, Gujarat

Alpa Sridhar* and Atul Patidar

Department of Geology, Faculty of Science, M.S. University of Baroda, Vadodara 390 002, India

The present communication is an attempt to study a point-bar deposit using Ground Penetrating Radar (GPR). The vertical as well as lateral variations in the lithofacies and the continuity of the bounding surfaces are delineated using the trench and GPR profiles. The basal part of the point-bar at Angad indicates deposition under a near-continuous flow with minor changes in velocity and direction giving rise to fining upward planar cross-stratified sand facies typical of a point-bar sequence. However, the sediments in the upper part show high degree of lateral and vertical heterogeneity in terms of facies development and is inferred to have resulted due to deposition by high stage flood events associated with cyclonic storms and the gradual waning flow. The lithofacies assemblage and morphology of the bar from head to tail-end suggest that the bar deposition is mainly controlled by downstream accretion. The sediment sequences of the point-bar exposed in trenches and on GPR profiles are helpful in deciphering the hydrologic regime of the depositing river channel.

THE Mahi River arises in the Malwa Plateau, Madhya Pradesh near Moripara and flows through the uplands and alluvial plain in Gujarat before debouching into the Gulf of Cambay (Figure 1). In the alluvial plain, it shows typical meandering river morphology and is characterised by the presence of extensive point-bars along its convex meander bends. Point-bar deposits accumulate in response to lateral and/or downstream migration of the river channel. The ability of the river to move and deposit sediment depends on stream competence, stream power, velocity of water, availability and size of sediments at peak discharge. Moreover, the flow conditions in fluvial systems having monsoon variability are complex as for the Mahi River. In such cases, the study of point-bar deposits becomes important as the fluctuations in the near-channel water level are manifested in the form of distinct sediment sequences. The variations in lithofacies in a point-bar complex can be related to the variability in discharge of the river in the near past, that is a function of seasonal flood events. In this context, these modern river deposits are well-studied elsewhere[1–4], however, in India, studies on these deposits have been initiated recently[5–9]. The basic hindrance in establishing the stratigraphy of a point-bar is the lack of lateral continuity in marking the lithofacies and characteristic bounding surfaces, since sections can be studied along trenches in a limited area. This problem can

*For correspondence. (e-mail: alpasridhar@rediffmail.com)

be addressed using imaging techniques, the Ground Penetrating Radar (GPR) being one of them. GPR imaging provides a continuous picture of the shallow subsurface stratigraphy and has been extensively used in understanding the fluvial environmental settings[10–12]. Some aspects of GPR such as instrument specification and physics are beyond the scope of this communication and readers can refer elsewhere for details[13–15].

Here we present the results of a GPR survey carried out over a point-bar deposit (Figure 2 *a*) and characterize its facies distribution, sequential evolution and correlate the lithofacies to the variance in discharge of the Mahi River resulting due to seasonal flood events on a small timescale. The Mahi River in Gujarat falls under the semi-arid climatic zone and the flow in the river is monsoon-related. Therefore, the channel has a pronounced low discharge period and a short flood period. The average annual rainfall over the Mahi River basin is 850 mm and the mean annual discharge is 382 m^3/s. The highest ever recorded level since 1959 (from when continuous gauged records are available) downstream of Wanakbori, a weir about 50 km upstream from Angad, was about 60 m in 1973 and the discharge[16] was 41208 m^3/s. The high flood level at Phajalpur just upstream of Angad (Figure 1 *b*) was 25 m and at Singrot (downstream of the present site), it was 19.82 m. The total suspended sediment load as measured at Kadana dam is about 1120 thousand metric tons during monsoon and 6.3 thousand metric tons during non-monsoon periods[16].

In the alluvial reaches of the Mahi River, each meander bend has a point-bar and a large portion of it is exposed at low flow level. The point-bar located on the left bank of the river near Angad was selected for this study (Figure 2 *a*). The channel bed is 200 m wide at low flow level and the flood plain, including the point-bar deposit extend here laterally for 500 m at the maximum curvature of the meander and 4.5 km longitudinally. Several distinct bars appear to have coalesced to form the present ridge and swale topography in the river bed near Angad. Three distinct topographic levels can be marked here. The lower level is about 1.5 m above the low flow level, and the second level, i.e. that of the exposed point-bar is 5 m above the low flow level. The third and the highest level which is up to about 15 m from the point-bar level is the terrace surface that has been assigned mid-late Holocene age by Maurya *et al.*[17].

The trench sections of the point-bar near Angad show a lot of heterogeneity in their upper parts (Figures 3 and 4). In all, five exposed sections were studied (Figure 3) along a single bar unit, one at the bar-head and two each in the intermediate zone and the tail end. The sediments were identified based on the classification proposed by Miall[18]. The base of the bar-head section comprises Sp facies, which is overlain by a 55 cm thick unit of Gp facies (Figure 3A). The Gp unit is overlain by a 10 cm horizontally bedded gravel layer; the top is marked by 30 cm thick Sp facies. Five second-order bounding surfaces separating distinct facies can be marked in this sequence (Figure 4 *a*). The second-order surfaces record boundaries within mesoform depos-

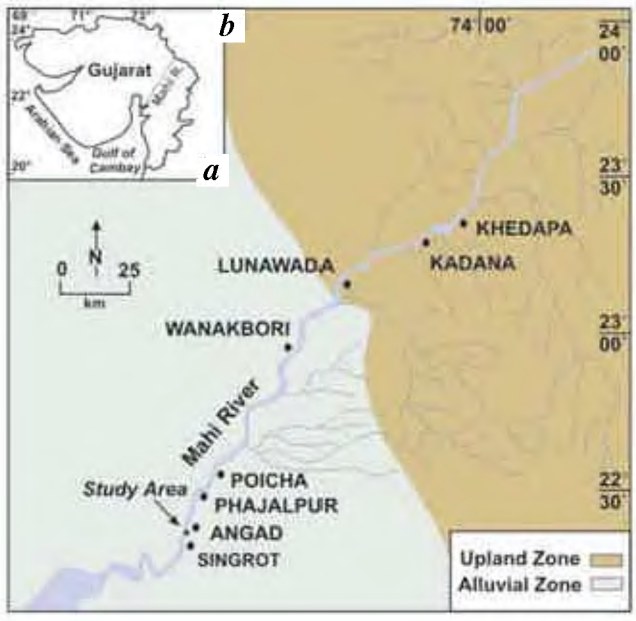

Figure 1. ***a***, Map showing location of Mahi River basin. ***b***, Mahi River basin with locations discussed in text. Geomorphic zones are after Rachna *et al.*[28].

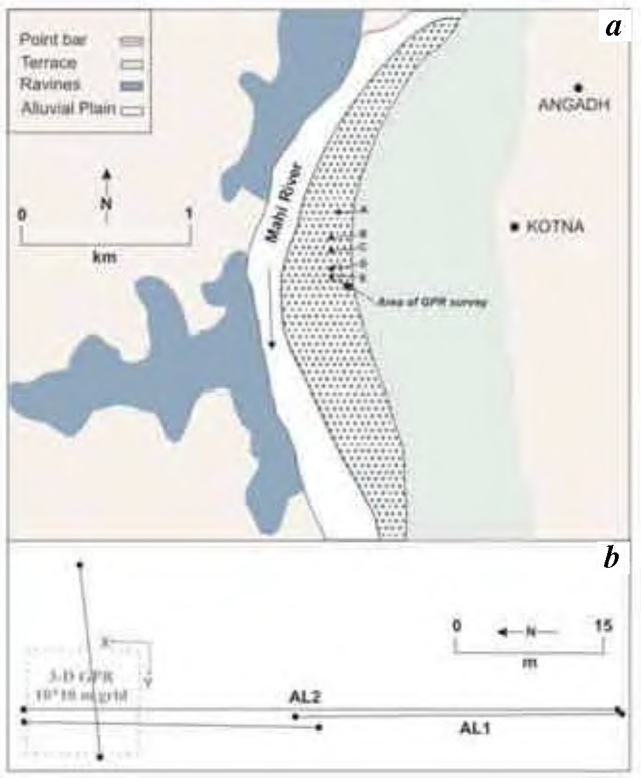

Figure 2. ***a***, Geomorphic setting around Angad point-bar. Locations of trench sections are marked from A–E. ***b***, Layout map of GPR survey showing position of transect lines (AL1 and AL2). Dashed square represents area of 3D survey.

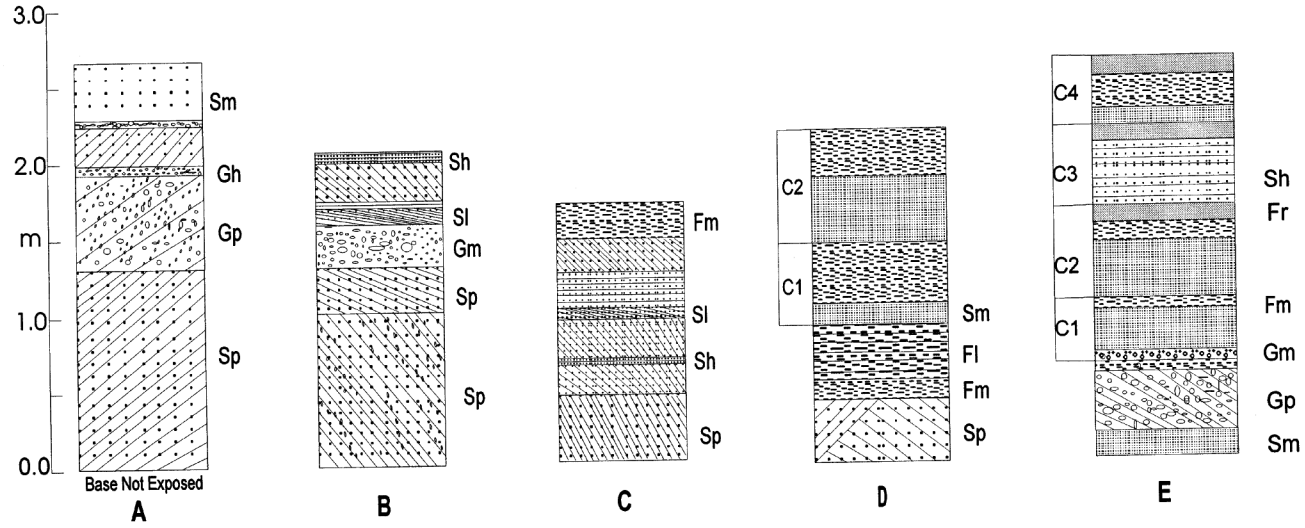

Figure 3. Measured trench sections (locations as in Figure 2 *a*) showing lithofacies assemblages (A, bar-head; B and C, intermediate zone; D and E, tail-end). Lithofacies after Miall[18] (Gp, Planar cross-bedded gravel; Gm, Massive gravel; Sp, Planar cross-bedded sand; Sh, Horizontal laminated sand; Sl, Low-angle cross-bedded sand; Sm, Massive sand; Fl, Fine laminated silt, mud; Fm, Massive silt mud; Fr, Massive root bioturbated mud, silt. C1–C4 are flood cycles.

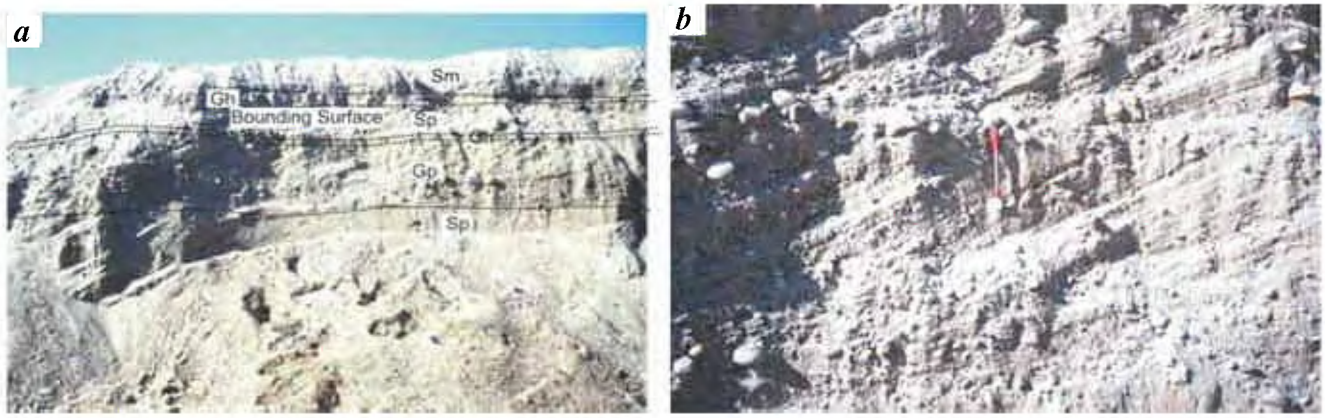

Figure 4. *a*, View of bar-head trench showing bounding surfaces and vertical variations in lithofacies. *b*, Close view of Gp facies showing coarser clasts.

its and represent a change in flow conditions but no significant time break[18]. The maximum clast size in this unit is in the range of 10–12 cm (Figure 4 *b*). The sections from the intermediate zone are predominantly comprised of sand facies either cross-stratified coarse sand (Sp) units with mud balls, gravels and shell, or horizontally laminated fine sand units (Sh, Figure 3 B, C). The presence of mud clasts in the Sp facies indicates reworking of the bottom clay drape unit and commencement of the next phase of deposition. Three units of upward fining lithofacies bounded by second-order surfaces are demarcated. The tail-end sections differ from the other sections in terms of preserved facies sequence (Figure 3 D, E). In these sections, the typical point-bar Sp facies is overlain by Fl and Fr facies which are separated by intermittent sand horizons.

The GPR imaging was carried out along several transects of the point-bar in this block to understand the heterogeneity in the sediment characteristics and lateral continuity. The instrument used for GPR survey was GSSI SIR-20 system with 200 MHz monostatic antenna. A calibrated survey wheel was attached with the antenna. To make the operation easy, positions of the transect lines were marked according to a pre-plan and the background noise creators were removed from the transect line (Figure 2 *b*). Several attempts were made to select the best acquisition parameters. All the profiles were acquired with 512 samples/scan and 16 bits/sample. Profiles AL1 and AL2 raised along the tail-end bar zone are best-suited for our survey objectives and are discussed at length later. The geophysical profiles gathered in one- and two-dimension provide a limited view of complex sedimentary deposits, but they can be viewed in real time to locate the interesting zones by 3D data acquisition. This step was followed to select our area of 3D interest from profile AL2 (2D GPR data). Profile AL2

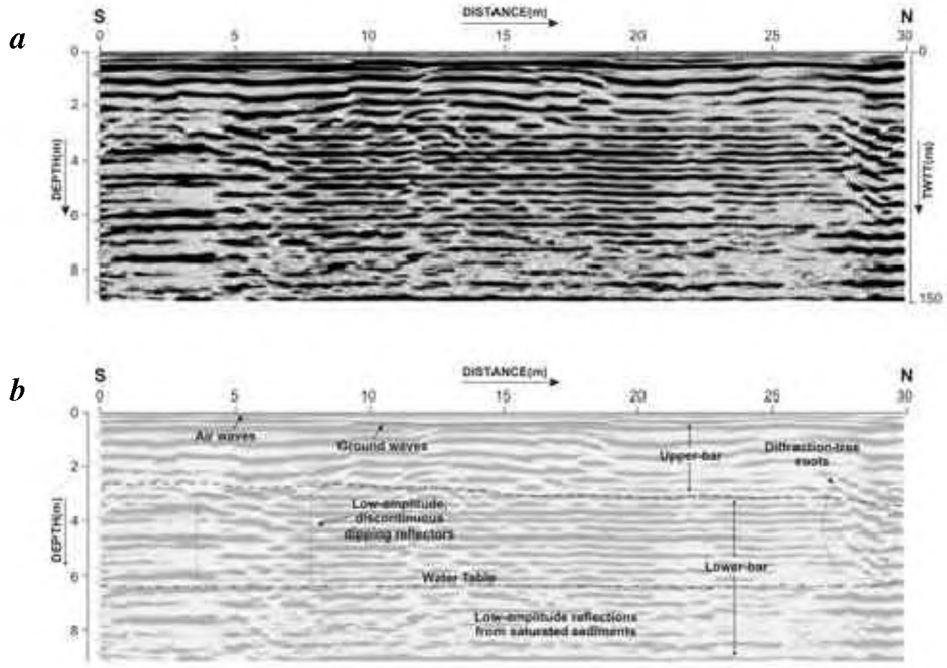

Figure 5. The 200 MHz radar data for line AL1 (see Figure 2 *b* for location). ***a***, Wiggle-mode representation of 30 m long GPR profile AL1. ***b***, Interpreted section of profile AL1 showing positions of air and ground waves. Broken line separates the upper-bar and lower-bar deposits. Low-amplitude, discontinuous dipping reflectors interpreted as bounding surfaces are marked in lower bar deposits. Water table is marked with dotted dashed line near 6.5 m depth. Note the changes in reflection strength from upper-bar sediments (unsaturated) and water-saturated sediments. Circled area marks high-angle diffraction due to tree roots.

showed some interesting zone near 45–60 m (distance axis) area and was selected for 3D profiling. The 3D data were collected from 10×10 m grid with 1m line interval and an odometer-based survey wheel was attached with the antenna. Software RADAN was used to improve the quality of data. The traces were edited wherever necessary. Distance Normalization Function and Static Correction Operation were performed to establish a constant horizontal scale and accurate depth calculation. The frequency spectrum was analysed and the cut-off frequencies were used to eliminate the interference. The lower frequency noise was removed using IIR (Infinite Impulse Response) filters. Stacking was applied to reduce the local interference and file length. GPR data show large-amplitude variations in heterogeneous medium. This problem was solved using AGC (Automatic Gain Control) function which averages the data, emphasizes the low amplitude signals and suppresses the high amplitude signals[19]. Display parameters were set to make the data in printable format. Interpretation of GPR profiles is based on correlation of radar reflections with corresponding trench logs. The correlation of trenches, vibracore and GPR data helps in evaluating the sedimentary succession[20].

AL1 is a 30 m long GPR profile (Figure 5 *a*) taken with dielectric constant 6 (~ 0.12 m/ns). Two uppermost high-amplitude continuous reflections occur due to direct air waves and ground waves respectively. The first continuous return occurs as the energy travels directly from transmitter to receiver through the air with high velocity (at near the speed of light, 2.998×10^8 m/ns). The next continuous returns occur due to the changes in dielectric properties of the medium (air to ground) and are not part of the stratigraphic data. Trenches and cut-bank exposures indicate a distinction between upper-bar (upper part of point-bar) and lower-bar deposits. The upper-bar deposits contain alternate horizons of fine sand and silty clay. This is also observed in profile AL1 (Figure 5 *b*), where the interfaces between upper-bar deposits are reflected with high-amplitude continuous returns till 2.5 m depth. The lower-bar deposits correspond to low- to moderate-amplitude discontinuous dipping reflectors. The dipping reflectors terminate at a laterally continuous, moderate-amplitude, near-horizontal reflector and are interpreted as a third-order bounding surface. Third-order surfaces develop at the top of minor bar sequences and are draped by mud facies indicating a falling velocity stage of water, following which the deposition of sediments resumes after a time lapse. These surfaces therefore are indicative of bar reactivation[18]. A distinct, continuous high-amplitude reflector is present at the position of the water table. Low-amplitude reflections below the water table are discontinuous and mark a water-saturated zone (Figure 5 *b*). The pattern of the reflectors suggests that the lower-bar facies continue below the water table up to a depth of 8 m at the base of the profile.

Similar reflectors continue further upstream as seen in the profile AL2, which is also a two-dimensional profile, 60 m in length and 5 m in depth (Figure 6 *a*). The continuity

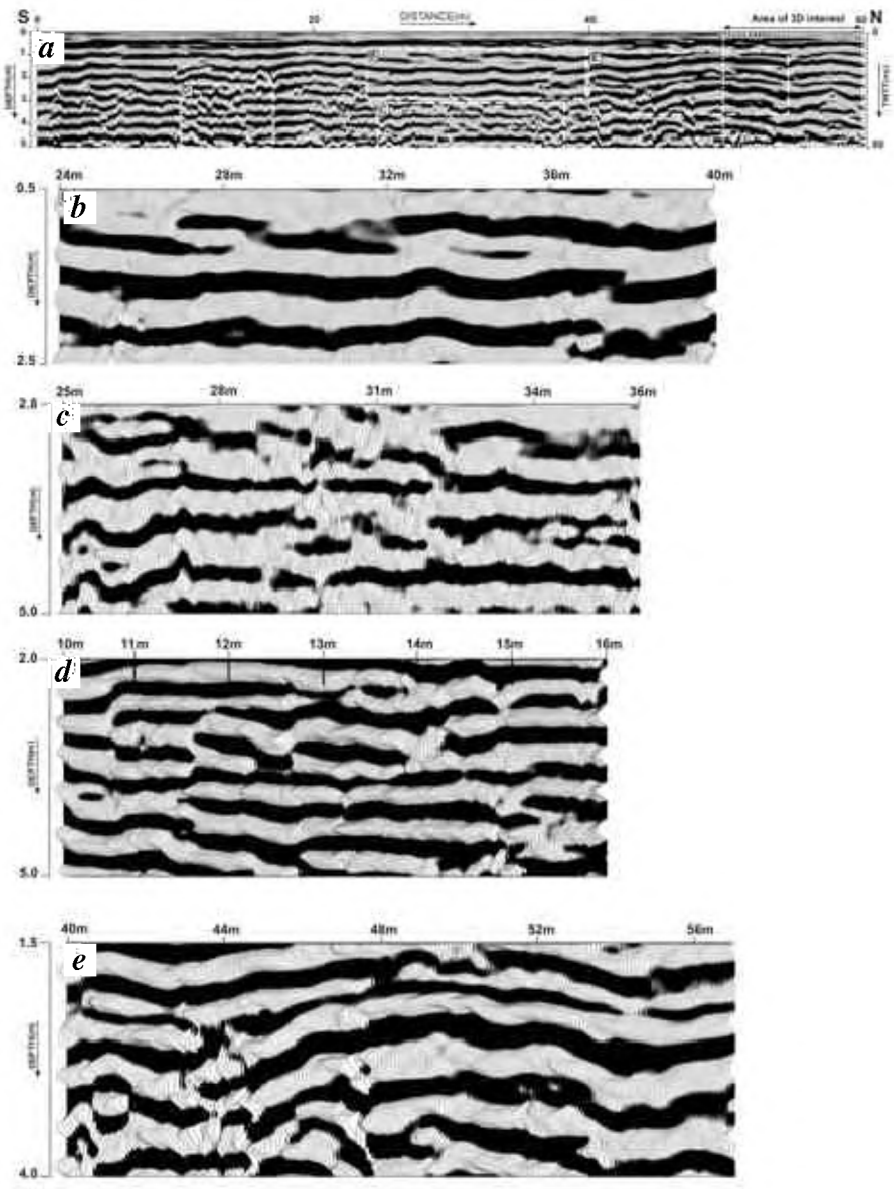

Figure 6. The 200 MHz radar data for line AL2 (see Figure 2 *b* for location). ***a***, A 60 m long interpreted GPR profile over the tail-end point-bar deposits at Angad. ***b–e***, The interpreted reflection patterns. Dotted square from 50 to 60 m represents the area of 3D interest. ***b***, Three high-amplitude continuous parallel reflections between 24 and 40 m marked as interfaces within the upper-bar deposits. ***c***, Low to moderate amplitude discontinuous parallel reflections from 25 to 36 m show minor sand lenses. ***d***, High-amplitude inclined reflections bounded by moderate amplitude reflections. ***e***, Moderate to low amplitude reflections from 40 to 57 m showing a mound-like structure, which is due to palaeo-topography of bar deposits (see Figure 7 *b* for lateral extension of these facies in *Y*-direction).

of air waves and ground waves is missing in this profile from 18 to 23 m and 38 to 43 m distance. This may be due to the changing surface conditions. Moisture variation in the sub-surface is a cause of discontinuity of the upper two reflectors[21]. Four types of reflector patterns are observed in this profile, marked here as continuous parallel, discontinuous parallel, oblique and mound shaped (Figure 6 *a*). The continuous patterns with high-amplitude and parallel reflections can be seen in Figure 6 *b*. The parallel reflections with constant thickness are sand and fine silt of upper bar. The discontinuous parallel reflections (Figure 6 *c*) are interpreted as minor sand inter-beds or lenses. The oblique facies (low-angle dipping reflections) indicate very coarse to coarse sand with medium-scale cross-strata bounded by third-order surfaces (Figure 6 *d*). Mound shaped reflections (Figure 6 *e*) which appear between 45 and 55 m (at distance axis), show a convex upward geometry. These reflections can be traced till the water table and are indicative of deposition over palaeo-topographic surface. The convex upward surface is the fourth-order bounding surface which demarcates the macro bed form top and points to downstream migration of the bar[18].

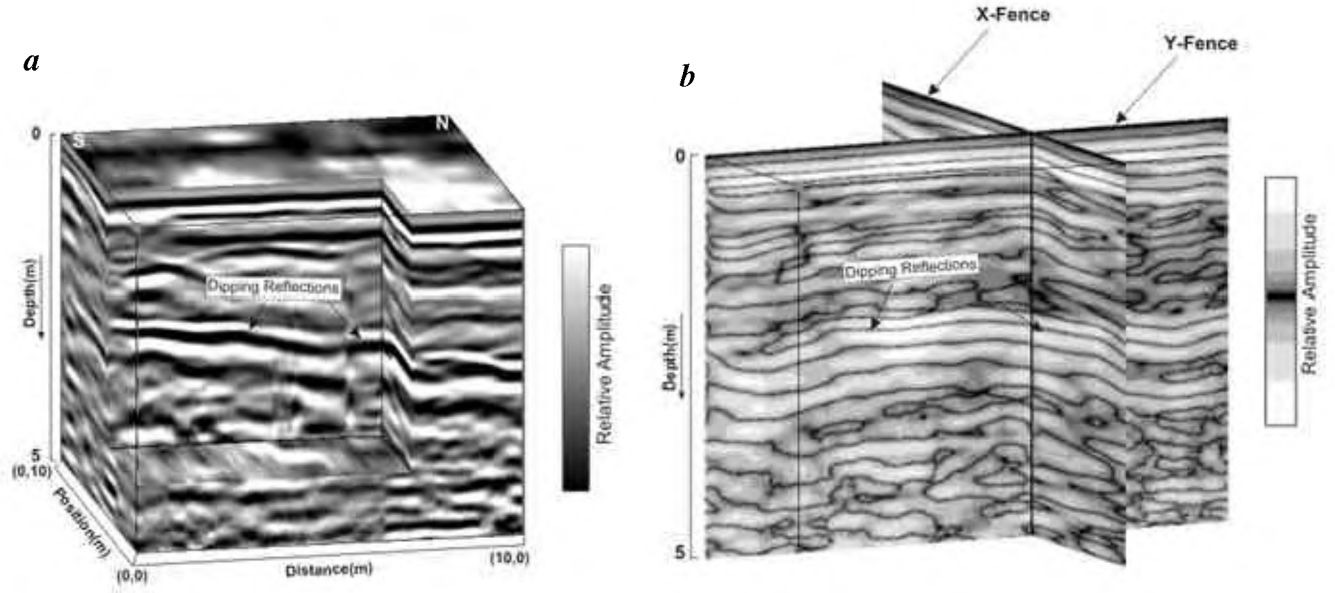

Figure 7. 3D GPR image of selected part of study area (see Figure 6 *a* for location). Profiles follow a 10 m × 10 m grid. ***a***, Data for cube were collected using 200 MHz-monostatic antenna attached with an odometer wheel. Image shows northward-dipping reflections near 3 m depth, which are interpreted as alternate facies of coarse sand and silt. ***b***, The *X*–*Y* fences selected from the 3D cube showing facies continuity in *X*-direction and their lateral extension in *Y*-direction. Tonal variation shows relative amplitude.

3D GPR profiles were acquired from a 10 m × 10 m grid with 80 ns time window which helped in interpreting the lateral extension of facies and their geometry. The cut-out 3D cube (Figure 7 *a*) shows northward-dipping facies in *X*-direction and their lateral extension in *Y*-direction. A fence presentation of 3D data (Figure 7 *b*) provides an overall view of internal pattern of sediment deposition. It is evident that the use of GPR has provided us with a more vivid picture of the continuity in the lithofacies and the bounding surfaces in all the three dimensions, which would otherwise not have been possible.

The variation in lithofacies in the trench sections and their continuity as seen in the GPR profiles point to a role of diverse depositional microenvironments in the development of the point-bar at Angad. Variation in the lithofacies that occurs in the bar-head and bar-tail deposits in a short stretch of less than a kilometre is striking. Bluck[22] has demonstrated that coarse bar deposits commonly develop preferentially in the upstream part of the bends and may migrate downstream. However, the deposition of predominantly coarse gravelly clasts at the bar-head, at an elevation of more than 3 m from the present low water level by a stream which normally carries fine load, can only be attributed to occasional high-stage flood event that may be associated with cyclonic storms. It has been documented that from 1891 to 1970, 49 monsoon depressions have traversed through this basin[23]. Crowley[24] related the coarsening upward sequence (Figure 3A) to the changing water velocity and depth over the bar crest during active bar growth due to downstream accretion. The rivers that have incised into alluvium have high banks and a small non-monsoonal flow channel, experience overbank flow only on few occasions and hence the fluvial activity is restricted within high banks[25].

In the intermediate zone (Figure 3B, C), where predominant sand facies are observed, the Sp facies made up of fine and coarse sand is interrupted by a unit of massive gravel representing plastic debris flow. The cross-stratified sand facies is seen overlying this gravel depicting a high flow and instantaneous settling, as is commonly seen in a flood event. Three cycles of fining upward sequences are interpreted at Angad and the end of each cycle is marked by the Sh facies. The horizontal or planar bed facies consisting of fine-to-medium sand may be attributed to an upper-flow regime plane bed condition, usually formed in shallow water near the top of the point-bar[26]. It is inferred that three distinct phases of current systems were operative in the deposition of the different cycles at Angad, the time gap, however, cannot be specified.

In the tail-end bar deposits, the Sp facies is readily differentiated from the overlying facies typical of waning flood events. In mixed load streams, the overbank deposits attain a considerable thickness and constitute a significant part of the upper point-bar sediments[27]. The sediment units in this sequence are massive or finely laminated, indicating only a partial preservation of the original flood sequence. The formation of horizontal laminations is attributed to upper flow regime during maximum flood. Clay drapes form at the end phase of the flood by the settling of suspended mud in places where local depressions stagnate flood waters. Four

such flood cycle deposits can be marked here (Figure 3E). The difference in the size of sediments in all the four cycles indicates that the intensity of the flood events depositing them was different. The silty clay units do show signatures of bioturbation and induration, suggesting that the unit was exposed for sometime before the next event of deposition occurred. The third- and fourth-order bounding surfaces suggest reactivation of deposition and accretion of the bar.

The preliminary results show that the point-bar lithofacies at Angad in the Mahi River basin show a lot of heterogeneity. The high frequency of low-order bounding surfaces indicates variability in the discharge levels of the Mahi River. There is a distinct trend of fining sediments from the bar-head to the bar-tail, suggesting three phases of accretion in the downstream direction. The sudden changes in the average grain size within dominantly sandy sequences may be taken as evidences of floods of variable energy. The point-bar does not show any evidence of lateral accretion and the presence of cut bank sections along these deposits suggests that the bar is currently being eroded. Detailed GPR imaging of point-bar has been helpful in tracing the continuity of downstream accretion surfaces, as also in demarcating sequences of unique flood events. The study further highlights the importance of point-bar deposits in understanding the changing hydrological conditions of a river basin and promises the use of GPR imaging.

1. Jackson II, R. G., Depositional model of point-bars in the Lower Wabash River. *J. Sediment. Petrol.*, 1976, **44**, 579–594.
2. Friend, P. F., Control of river morphology by the grain size of sediment supplied. *Sediment. Geol.*, 1993, **85**, 171–177.
3. Weerts, J. T. and Bierkens, F. P., Geostatistical analysis of overbank deposits of anastomosing and meandering fluvial systems; Rhine-Meuse Delta, The Netherlands, *Sediment. Geol.*, 1993, **85**, 212–232.
4. Santos, M. L. and Stevaux, J. L., Facies and architectural analysis of channel sandy macroforms in the upper Parana river. *Quat. Int.*, 2000, **72**, 87–94.
5. Tewari, R. C. and Gaur, R. P., Structures and sequences in fine-grained point-bars of Yamuna River near Etawah, Uttar Pradesh, *J. Geol. Soc. India*, 1991 **39**, 647–679.
6. Shukla, U. K., Singh, I. B., Srivastava, P. and Singh, D. C., Palaeocurrent patterns in braid and point-bar deposits: Examples from Ganga river, India. *J. Sediment. Res.*, 1991, **69**, 992–1002.
7. Singh, I. B., Shukla, U. K., Srivastava, P., Point-bar complex of an exhumed channel in upland interfluve of Ganga Plain. *J. Geol. Soc. India*, 1998, **51**, 315–322.
8. Tiwari, G. S., Tiwari, R. N. and Singh, K. N., Vertical successions of channel bar, point-bar and natural levee deposits, Ganga and Yamuna River, Allahabad, UP. *J. Geol. Soc. India*, 2004, **64**, 305–316.
9. Shukla, U. K. and Singh, I. B., Signatures of palaeofloods in sand-bar–levee deposits, Ganga Plain, India. *J. Geol. Soc India*, 2004, **64**, 455–460.
10. Jol, H. M. and Smith, D. G., Ground penetrating radar of northern lacustrine deltas. *Can. J. Earth Sci.*, 1991, **28**, 1939–1947.
11. Van Overmeeren, R. A., Radar facies of unconsolidated sediments in the Netherlands: A radar stratigraphy interpretation method for hydrogeology. *J. Appl. Geophys.*, 1998, **40**, 1–18.
12. Neal, A., Pontee, N. I., Pye, K. and Richards, J., Internal structure of mixed-sand-and-gravel beach deposits revealed using ground-penetrating radar. *Sedimentology*, 2002, **49**, 789–804.
13. Davis, J. L. and Annan, A. P., Ground-penetration radar for high resolution mapping of soil and rock stratigraphy. *Geophys. Prospect.*, 1989, **37**, 531–551.
14. Kruk, J. V. D. and Slob, E. C., Reduction of reflection from above surface objects in GPR data. *J. Appl. Geophys.*, 2004, **55**, 271–278.
15. Maurya, D. M. *et al.*, Need for initiating ground penetrating radar studies along active faults in India: An example from Kachchh. *Curr. Sci.*, 2005, **88**, 231–240.
16. CWC, Water and related statistics. Central Water Commission, New Delhi, 1996.
17. Maurya, D. M., Malik, J. N., Raj, R. and Chamyal, L. S., The Holocene valley, fill terrace on the lower Mahi valley, Gujarat. *Curr. Sci.*, 1997, **73**, 539–542.
18. Miall, A. D., Architectural element analysis. A new method of analysis applied to fluvial deposits. *Earth Sci. Rev.*, 1985, **22**, 261–308.
19. Annan, A. P., Practical processing of GPR data. *Sensors Software*, 1999.
20. Bridge, J. S., Alexander, J., Collier, R. E. L., Gawthorpe, R. L. and Jarvis, J., Ground Penetrating Radar and coring used to study the large-scale structure of point-bar deposits in three dimensions. *Sedimentology*, 1995, **42**, 839–852.
21. Moorman, B. J., Judge, A. S. and Smith, D. G., Examining fluvial sediments using ground penetrating radar in British Columbia. *Geol. Surv. Can.*, 1991, **91**, 31–36.
22. Bluck, B. J., Sedimentation in the meandering river Endrick., *Scott. J. Geol.*, 1971, **7**, 93–138.
23. Dhar, O. N., Rakhecha, P. and Sangam, R. B., A study of major rainstorms over and near Mahi basin up to Kadana dam site for the evaluation of probable maximum design storm. *J. Power River Valley Dev.*, 1975, **25**, 29–35.
24. Crowley, K. D., Large scale bed configurations (Macroforms), Platte river basin, Colorado and Nebraska: Primary structures and formative processes. *Geol. Soc. Am. Bull.*, 1983, **94**, 117–133.
25. Kale, V. S., Geomorphic effects of monsoon floods on Indian Rivers. *Nat. Hazards*, 2003, **28**, 65–84.
26. Harms, J. C. and Fahnestock, R. K., Stratification bedforms and flow phenomena. *Soc. Econ. Paleontol. Mineral., Spec. Publ.*, 1965, **12**, 84–115.
27. Ray, P., Structure and sedimentological history of the overbank deposits of a Mississippi river Point bar. *J. Sediment. Petrol.*, 1976, **46**, 788–801.
28. Rachna, R., Maurya, D. M. and Chamyal, L. S. Tectonic Geomorphology of the Mahi River basin, Western India. *J. Geol. Soc. India*, 1999, **54**, 387–398.

ACKNOWLEDGEMENTS. We thank Prof. L. S. Chamyal for help and guidance and for permission to use GPR. We also thank to Drs D. M. Maurya, Rachna Raj, Subhash Bhandari and Naresh Mulchandani for help in carrying out GPR survey. Financial assistance provided by DST, New Delhi to A.S. is acknowledged.

Received 22 January 2005; revised accepted 25 April 2005